JOURNAL OF GEOPHYSICAL RESEARCH, VOL. 115, B00B03, doi:10.1029/2009JB006970, 2010

Ground surface deformation patterns, magma supply, and magma storage at Okmok volcano, Alaska, from InSAR analysis: 2. Coeruptive deflation, July–August 2008

Zhong Lu[1,2] and Daniel Dzurisin[1]

Received 9 September 2009; revised 20 November 2009; accepted 17 December 2009; published 5 May 2010.

[1] A hydrovolcanic eruption near Cone D on the floor of Okmok caldera, Alaska, began on 12 July 2008 and continued until late August 2008. The eruption was preceded by inflation of a magma reservoir located beneath the center of the caldera and ~3 km below sea level (bsl), which began immediately after Okmok's previous eruption in 1997. In this paper we use data from several radar satellites and advanced interferometric synthetic aperture radar (InSAR) techniques to produce a suite of 2008 coeruption deformation maps. Most of the surface deformation that occurred during the eruption is explained by deflation of a Mogi-type source located beneath the center of the caldera and 2–3 km bsl, i.e., essentially the same source that inflated prior to the eruption. During the eruption the reservoir deflated at a rate that decreased exponentially with time with a $1/e$ time constant of ~13 days. We envision a sponge-like network of interconnected fractures and melt bodies that in aggregate constitute a complex magma storage zone beneath Okmok caldera. The rate at which the reservoir deflates during an eruption may be controlled by the diminishing pressure difference between the reservoir and surface. A similar mechanism might explain the tendency for reservoir inflation to slow as an eruption approaches until the pressure difference between a deep magma production zone and the reservoir is great enough to drive an intrusion or eruption along the caldera ring-fracture system.

Citation: Lu, Z., and D. Dzurisin (2010), Ground surface deformation patterns, magma supply, and magma storage at Okmok volcano, Alaska, from InSAR analysis: 2. Coeruptive deflation, July–August 2008, *J. Geophys. Res.*, *115*, B00B03, doi:10.1029/2009JB006970.

1. Introduction

[2] An eruption at Okmok volcano started on 12 July 2008 and ended in late August 2008 [*Larsen et al.*, 2009]. The eruption differed from previous eruptions during the past century in several respects. First, the 2008 eruption started from the northwest flank of Cone D (altitude of 780 m) [*Larsen et al.*, 2009], whereas earlier eruptions were from Cone A (altitude of 900 m) (Figure 1). Second, the 2008 eruption was explosive and hydrovolcanic in nature, indicating strong magma interactions with groundwater and surface water. In contrast to earlier eruptions that produced basaltic lava flows, the 2008 eruption was noneffusive; instead, it blanketed much of the caldera and adjacent landscape with fine-grained tephra. Finally, unlike earlier eruptions, the 2008 eruption created and modified several lakes in the northeastern part of the caldera (Figures 1c and 1d).

[3] Deformation of Okmok volcano prior to and since its 1997 eruption has been studied systematically, using both interferometric synthetic aperture radar (InSAR) images [e.g., *Lu et al.*, 1998, 2000, 2005, 2010; *Mann et al.*, 2002] and GPS measurements [*Miyagi et al.*, 2004; *Fournier et al.*, 2009]. The volcano inflated at a generally declining rate prior to its 1997 eruption, deflated rapidly during the eruption, and resumed inflating several months thereafter at a rate that varied over time from summer 1997 to 10 July 2008 [*Lu et al.*, 2005, 2010; *Fournier et al.*, 2009] (Figure 2a). Inversion of the surface deformation data shows that the horizontal position of the center of a magma storage zone that underlies Okmok caldera at ~3.0 km below sea level (bsl) remained nearly stationary from 1997 to 2008 [*Lu et al.*, 2005, 2010; *Fournier et al.*, 2009]. InSAR images show that the maximum surface uplift rate prior to either eruption was ~20 cm/y during 2002–2003; minimum inflation rates of 2–5 cm/y occurred during 1993–1995 and 2005–2006. Subsidence of a few centimeters was observed during 1995–1996 before the 1997 eruption, and also during 2004–2005 before the 2008 eruption (Figure 2a). InSAR analysis shows that 10–15 cm of surface uplift occurred from summer 2007 to summer 2008, and that no significant short-term precursory deformation occurred immediately before the 12 July 2008 eruption [*Lu et al.*, 2010]. The temporal pattern of inflation revealed by

[1] Cascades Volcano Observatory, U.S. Geological Survey, Vancouver, Washington, USA.
[2] EROS Center, U.S. Geological Survey, Vancouver, Washington, USA.

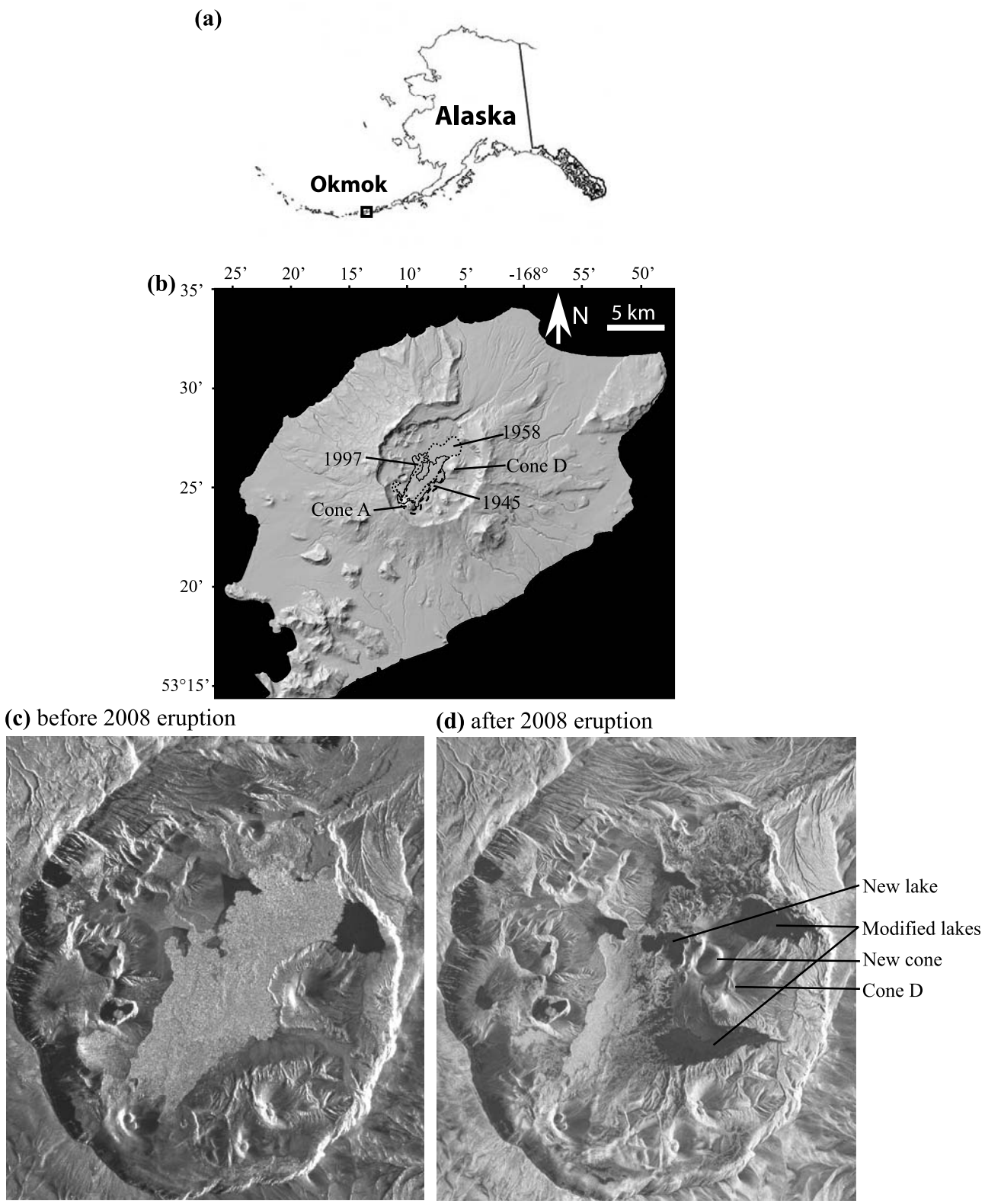

Figure 1. (a) Location of Okmok volcano in the central Aleutian volcanic arc; (b) shaded relief image of Okmok volcano, showing intracaldera Cones A and D, and lava flows emplaced in 1945, 1958, and 1997; (c) Radarsat-1 SAR intensity image of Okmok caldera before the 2008 eruption; and (d) TerraSAR-X SAR intensity image of Okmok caldera after the 2008 eruption. Notice changes in the northeastern part of the caldera, a new cone northwest of Cone D, a new lake, and old lakes modified by the 2008 eruption.

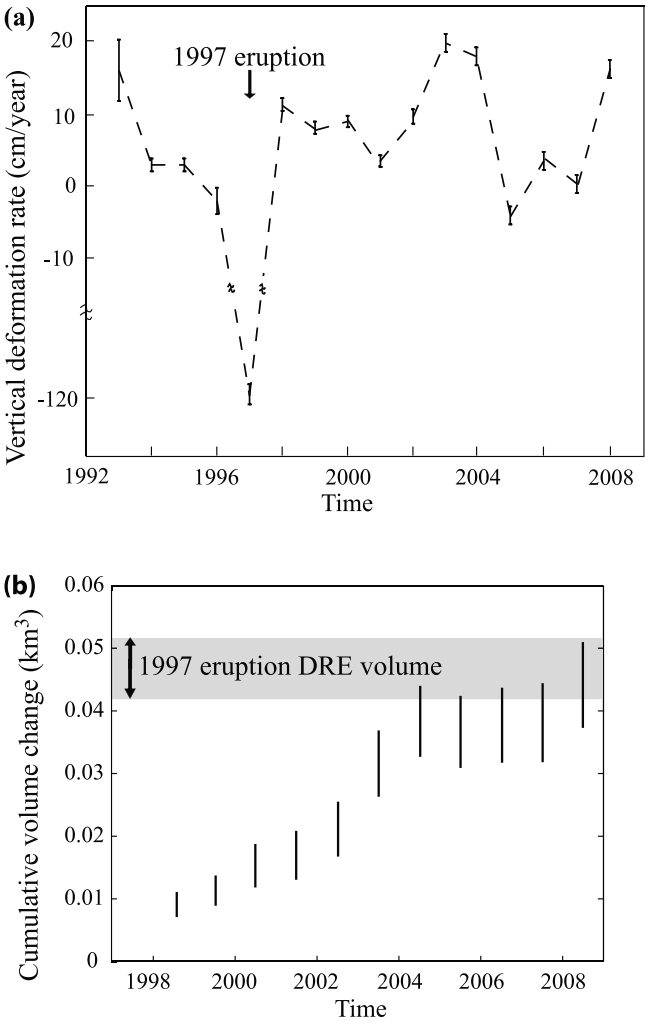

Figure 2. (a) Annual maximum vertical deformation derived from modeling multiple temporal InSAR images [*Lu et al.*, 2010] and (b) cumulative magma supply to the shallow reservoir beneath Okmok volcano from 1992 to 10 July 2008, 2 days prior to the 12 July 2008 eruption, inferred from InSAR analysis. See text for details.

InSAR imagery is consistent with continuous GPS (CGPS) observations for the same time period [*Fournier et al.*, 2009]. The net increase in volume of the magma reservoir from the end of the 1997 eruption to the start of the 2008 eruption is comparable to the decrease in reservoir volume during the 1997 eruption, i.e., 0.047 ± 0.005 km^3 [*Lu et al.*, 2005, 2010] (Figure 2b). By 10 July 2008, 85–100% of that volume had been replenished, presumably by magma from a deep source [*Lu et al.*, 2010].

[4] This paper is focused on mapping, analysis, and modeling of ground surface deformation during the 2008 eruption at Okmok as revealed by time-sequential InSAR images. We first describe the SAR data used for this study and advanced InSAR methods used to analyze the deformation, including correction for topography-induced range offsets and multiple aperture radar InSAR processing. Then we model the coeruption interferograms and derive changes in reservoir volume as a function of time. Finally, we discuss implications of the 2008 eruption results for Okmok's magma plumbing system.

2. InSAR Data and Analysis

2.1. SAR Data

[5] To study ground surface deformation that occurred during the 2008 Okmok eruption, we obtained SAR images from 5 different satellite sensors: the European Environmental Satellite (Envisat), European Remote sensing Satellite 2 (ERS-2), Canadian Radar Satellite 1 (Radarsat-1), Japanese Advanced Land Observing Satellite (ALOS) Phased Array type L band SAR (PALSAR), and German TerraSAR-X (Table 1). These multiple temporal SAR images were acquired in 3 different wavelength (λ) domains: L band (λ = 236.2 mm) for ALOS, C band (λ= 56.3 mm) for Envisat and C band (λ= 56.6 mm) for Radarsat-1 and ERS-2, and X band (λ= 31.1 mm) for TerraSAR-X. The SAR images were acquired at different radar look angles ranging from 20.5° to 41.2° from vertical, and along both descending (when satellites travel from north to south) and ascending (south to north) tracks (Table 1). The original resolutions of the images are ~5 m for TerrSAR-X, ~8 m and ~16 m for ALOS, and ~25 m for Envisat, ERS-2, and Radarsat-1.

[6] We used a 1 arc second digital elevation model (DEM) from the Shuttle Radar Topography Mission (SRTM) to create deformation interferograms from suitable pairs of SAR images (Table 1). Both conventional two-pass InSAR processing [*Massonnet and Feigl*, 1998; *Zebker et al.*, 1994; *Rosen et al.*, 2000] and advanced InSAR processing techniques (see below) were exploited to improve the quality of the deformation maps.

2.2. InSAR Processing: Improved Technique for Long Baseline Image Pairs

[7] A stringent prerequisite in InSAR processing is the precise registration of reference and slave SAR images and resampling the slave image to the geometry of the reference image. For conventional InSAR processing, coregistration is done by cross correlating the reference and slave images at a dense grid of pixel locations and using the results to construct range and azimuth offset polynomials for the entire image. The range and azimuth offset polynomials are expressed as functions of range and azimuth pixel position. A problem arises when, for an interferogram with a large perpendicular baseline, topographic variations introduce additional localized offsets between the reference and slave images [e.g., *Sandwell et al.*, 2008]. The range offset due to topographic relief is linearly dependent on topography and can be approximated as

$$\Delta r_{off} = -\frac{B_\perp}{H \tan\theta}\Delta h, \tag{1}$$

where Δr_{off} is the range offset due to height difference Δh, $B_\perp$ is the perpendicular baseline of the interferogram, H is the altitude of the satellite above Earth, and θ is the SAR look angle. For the Envisat SAR sensor, normal values for H and θ are about 790 km and 23° (beam mode IS2), respectively. A 1 km difference in topography (a typical value for Aleutian volcanoes including Okmok) can induce about ~1.5 m range offset for an Envisat interferogram

Table 1. InSAR Data and Imaging Characteristics[a]

Date 1	Date 2	$B_\perp$(m)	Sensor	SAR Look Angle (°)	Satellite Track Number/Angle (°)	Wavelength (mm)
20071007	20080713	97	Envisat	20.5	179/−13.4	56.3
20071010	20080716	−5	Envisat	25.5	222/−13.4	56.3
20070913	20080724	−275	Envisat	24.0	344/−166.7	56.3
20080619	20080724	−71	ERS-2	24.0	344/−166.7	56.6
20080627	20080801	−69	Envisat	23.0	451/−13.3	56.3
20080710	20080803	−119	Radarsat-1	33.5	ASC/−11.3	56.6
20070905	20080820	8	Envisat	25.5	222/−13.4	56.3
20080724	20080828	19	Envisat	24.0	344/−166.7	56.3
20070921	20080905	70	Envisat	23.0	451/−13.3	56.3
20080801	20080905	676	Envisat	23.0	451/−13.3	56.3
20071002	20080916	−266	Envisat	21.5	115/−166.8	56.3
20080713	20080921	−118	Envisat	20.5	179/−13.4	56.3
20080716	20080924	−186	Envisat	25.5	222/−13.4	56.3
20070822	20081007	−3876	PALSAR	38.7	300/−10.2	236.2
20080801	20081010	−224	Envisat	23.0	451/−13.3	56.3
20080914	20080925	83	TerraSAR-X	41.2	ASC/41.2	31.1

[a]Date format used here is yyyymmdd (read 20071007 as 7 October 2007).

with a perpendicular baseline of 500 m. This offset is about 8% of the range pixel size. For the ALOS PALSAR sensor, normal values for H and θ are about 700 km and 34°, respectively. The topography-induced range offset for a fine beam PALSAR interferogram with a perpendicular baseline of 1 km can be as large as ~2.1 m, or about 23% of the range pixel size. In other words, range offsets due to topographic relief at Okmok can be large enough to degrade InSAR coherence if the offsets are not taken into account during image coregistration. We used a DEM and the SAR imaging geometry to compute direct functions that map the position of each pixel in the reference image to a corresponding pixel location in the slave image. This results in significant improvement in coherence for interferograms with relatively large baselines.

[8] To illustrate the improvement in InSAR coherence obtained by accounting for topography-induced range offsets, we used an ALOS PALSAR interferogram with a perpendicular baseline of 3876 m (Table 1 and Figure 3). Topographic relief of 1 km produces a range shift of about 8 m for a baseline of this length. We compared an unfiltered interferogram produced using conventional InSAR processing (Figure 3a) with an unfiltered interferogram that takes into account the range offset due to topography (Figure 3b). Improved coherence in the second case is evidenced by better defined interferometric fringes on Okmok's western flank, and by a coherence histogram for that area (Figure 3c). This method, although effective for avoiding potential coherence loss caused by topography-induced range offsets, will not improve coherence if the loss is due to temporal decorrelation. For example, coherence loss within the caldera and on the eastern flank of Okmok (Figures 3a and 3b), which was caused by geomorphic changes and ashfall during the 2008 eruption, cannot be mitigated by this technique.

[9] Figure 4 shows several interferograms that span part or all of the 2008 eruption. The SAR images used to create the interferograms are from different satellites (Envisat, ERS-2, Radarsat-1, and ALOS) with different imaging geometries. Figure 4a shows an Envisat interferogram that spans the period 7 October 2007 to 13 July 2008, which includes the first 13 hours of the eruption. This is the most coherent InSAR image acquired during the entire eruption. In interferograms that end after 13 July 2008, coherence was maintained in the western half of the caldera but lost in the eastern half of the caldera and on the eastern flank of the volcano. Loss of coherence was caused primarily by explosions and melting snow/ice, as well as volcanic ash that blanketed the eastern half of the volcano during the first several hours of the eruption. The maximum line-of-sight (LOS) range change indicated by the interferogram is ~75 cm. The sense of motion is such that the center of the caldera moved away from the satellite, i.e., the center of the caldera moved down as the volcano deflated. Figure 4b shows another ascending track Envisat interferogram that spans 10 October 2007 to 16 July 2008; the end time is 3.5 days after the onset of the 2008 eruption. The total LOS range change during this period is ~115 cm in a caldera down sense (deflation). Figure 4c shows an interferogram formed from descending ERS-2 images acquired on 19 June 2008 and 24 July 2008. Coherence inside the caldera is worse in this case than in the earlier InSAR images owing to eruption effects. All of the InSAR images formed with data acquired after 24 July 2008 (e.g., Figures 4d–4h) are not coherent inside the caldera, suggesting significant morphological changes due to explosions, new ash deposits, collapse owing to groundwater changes, and redistribution of surface water [*Larsen et al.*, 2009]. Coherent fringes outside the caldera in post-24 July 2008 interferograms indicate that the total amount of deflation increased with time as the eruption proceeded (Figures 4d–4h).

2.3. Multiple Aperture Radar InSAR Processing

[10] The conventional approach to measuring along-track displacements near the deformation center is to use image correlation to map the pixel offset field, which can be done to an accuracy of about 1/10 of the pixel size (~5 m). *Bechor and Zebker* [2006] introduced a multiple aperture InSAR (MAI) technique, which was improved by *Jung et al.* [2009], to produce along-track displacement images that represent a remarkable improvement over the pixel offset tracking method. An MAI along-track displacement map can be combined with InSAR deformation images from descending and ascending image pairs to produce a full three-dimensional displacement map [*Jung et al.*, 2010]. MAI utilizes subaperture processing techniques to create one forward-looking single-look complex (SLC) image and

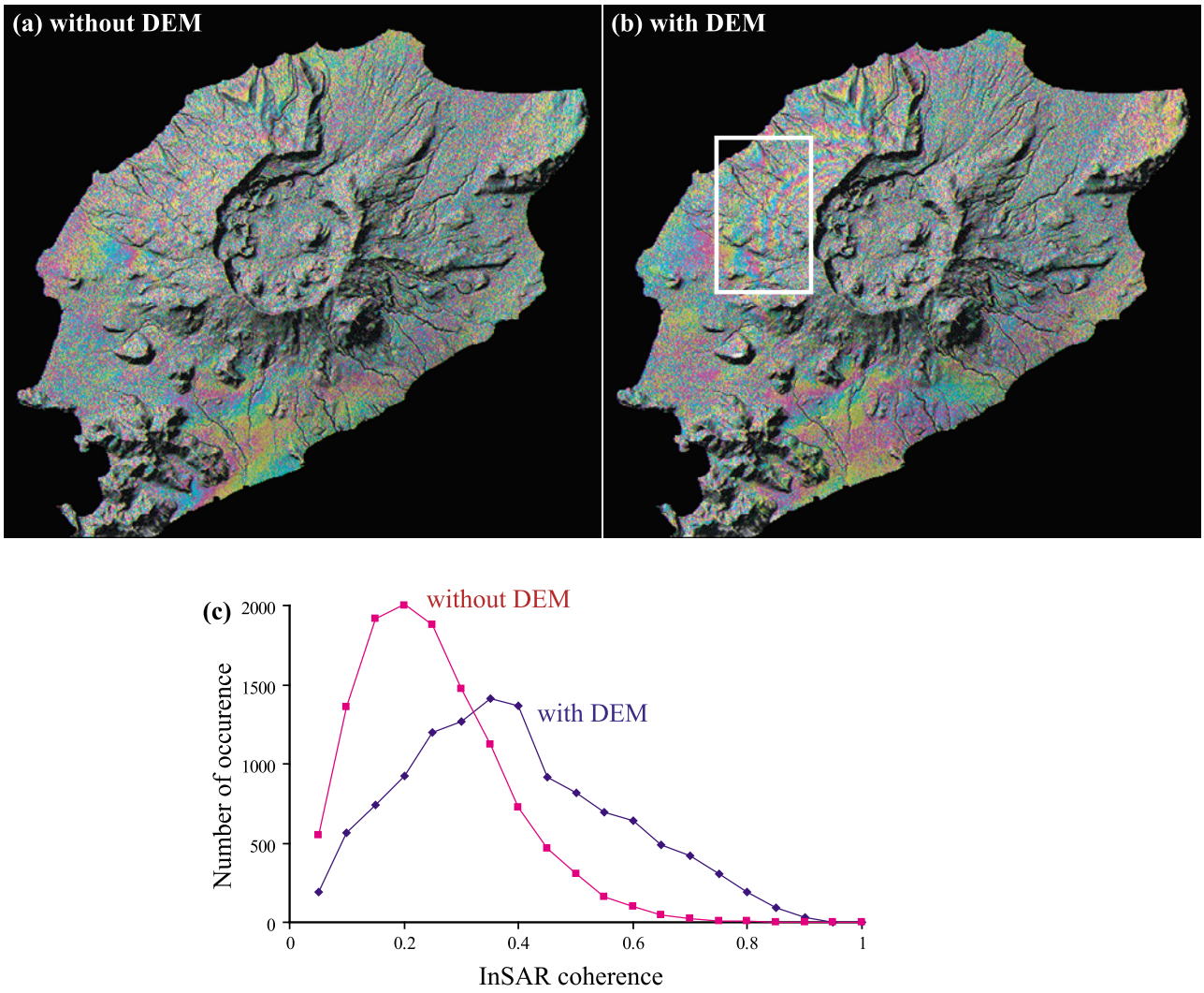

Figure 3. Interferograms formed (a) with and (b) without taking into account the effect of topography during image registration and resampling of the SAR images. (c) Histograms of InSAR coherence within the area outlined by the white rectangle in Figure 3b. Rightward shift of the distribution maximum for the interferogram that includes topographic effects (blue line) relative to the uncorrected interferogram (red line) indicates the coherence improvement by ~0.2 in the corrected interferogram.

one backward-looking SLC image from raw SAR data. Two raw SAR data sets processed in this way are used to form one forward-looking and one backward-looking interferogram from the corresponding SLC images. The phase difference between the forward-looking and backward-looking interferograms is an MAI image that shows ground surface displacements in the azimuth (i.e., along track) direction, which is approximately north-south for all operational SAR satellites.

[11] We applied MAI processing to the InSAR image (Figure 4a) that brackets the first 13 hours of the 2008 Okmok eruption to prospect for along-track surface deformation associated with rifting or dike opening, which commonly occurs during effusive eruptions. For the Envisat satellite, the effective antenna length is about 10 m. We used 50% of the full aperture width for MAI processing. Based on the relationship between the MAI phase and the effective antenna length [*Bechor and Zebker*, 2006; *Jung et al.*, 2009], one MAI fringe in Figure 5a corresponds to 10 m along-track displacement. Examination of MAI phase measurements outside the caldera suggests that the standard deviation of the along-track displacement measurements is ~15 cm (Figure 5b). In the center of the caldera where coherence was maintained, the MAI image indicates no significant north-south surface displacement during the first 13 hours of the 2008 eruption. We calculated the predicted displacement caused by a vertical dike striking in the direction from Cone A to Cone D (southwest to northeast). If the 2008 eruption was fed by such a dike, it would have to be less than ~3 km in length with an opening of less than ~50 cm to escape detection by InSAR and MAI images as well as CGPS measurements [*Freymueller et al.*, 2008]. Given the theoretical calculation, the MAI result, and the goodness of fit to the coeruption interferograms

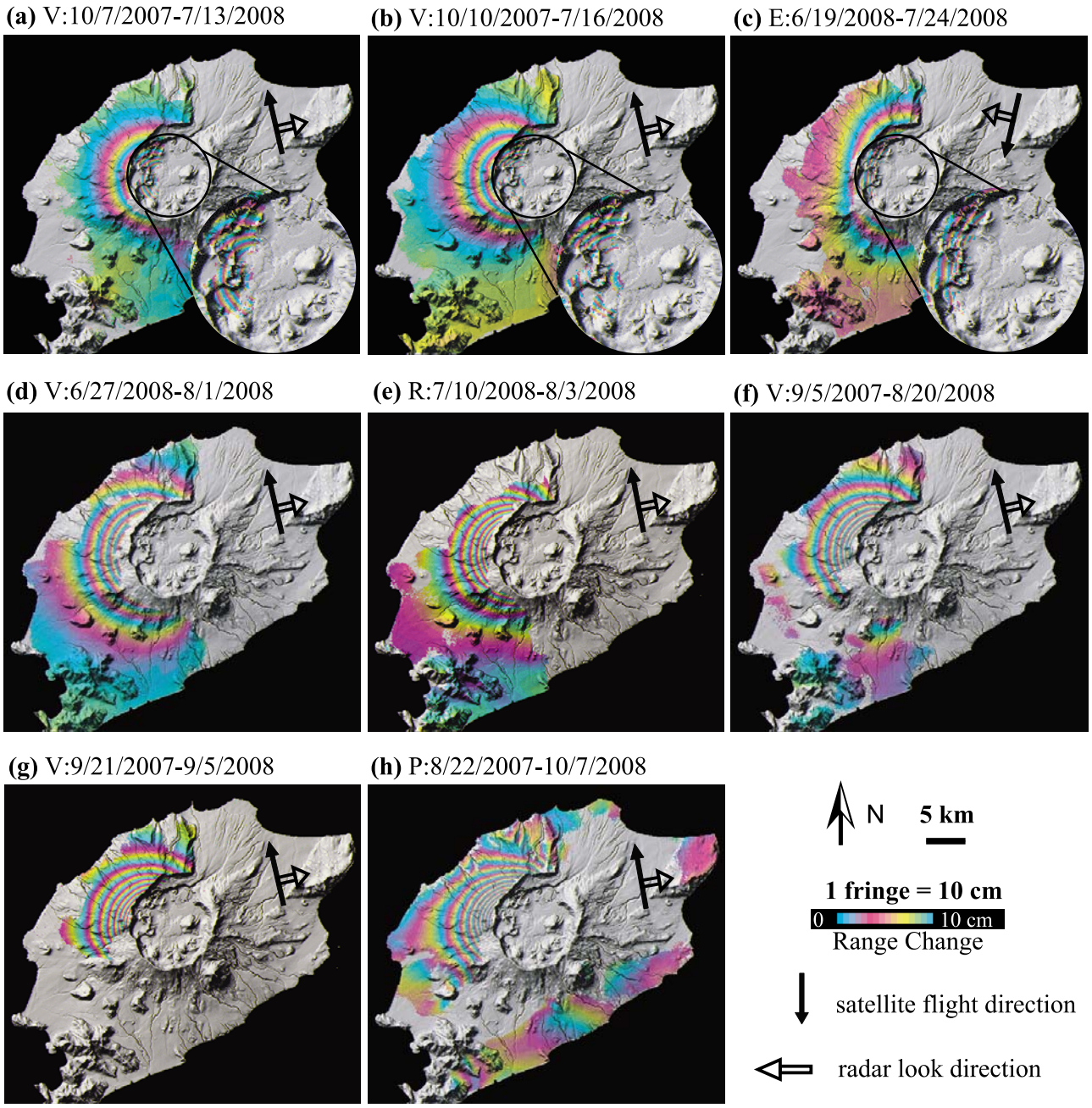

Figure 4. Examples of multitemporal deformation interferograms that span the 2008 eruption (Table 1). InSAR image dates are as follows (date format here is yyyymmdd): (a) 20071007–20080713 (Envisat Track 179), (b) 20071010–20080716 (Envisat Track 222), (c) 20080619–20080724 (ERS-2 Track 344), (d) 20080627–20080801 (Envisat Track 451), (e) 20080710–20080803 (Radarsat-1 ascending track), (f) 20070905–20080820 (Envisat Track 222), (g) 20070921–20080905 (Envisat Track 451), and (h) 20070922–20081007 (PALSAR Track 300). To better illustrate the large amount of coeruptive deformation and to facilitate intercomparison of the images, one fringe (color cycle) is used to represent 10 cm of line-of-sight (LOS) ground motion in all cases. Deformation inside the caldera (Figures 4a–4c) is enlarged in the inset to improve visibility. Areas that lack interferometric coherence are uncolored. Satellite ID (E is ERS-2, R is Radarsat-1, V is Envisat, and P is PALSAR), image acquisition dates, satellite flight direction, and radar look direction are labeled.

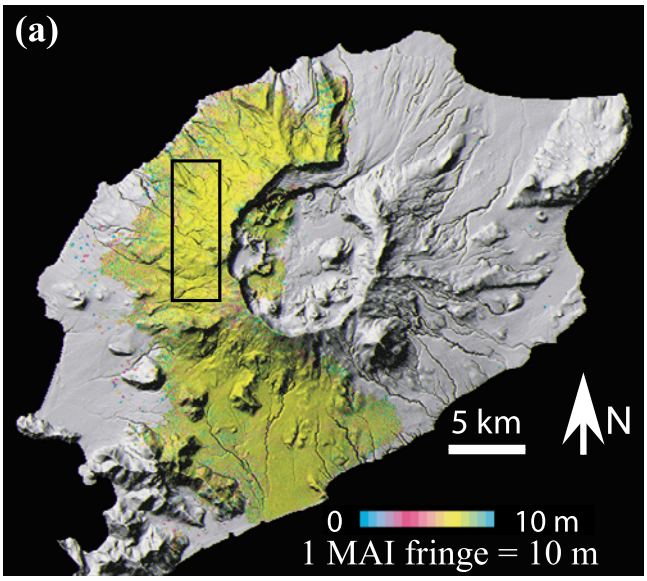

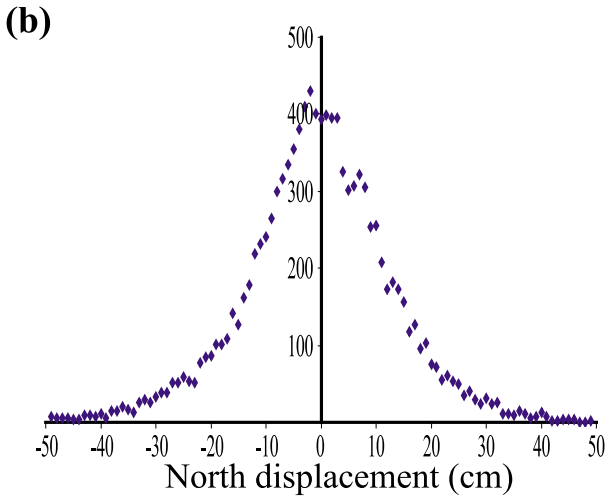

Figure 5. (a) MAI interferogram (7 October 2007 to 13 July 2008) that spans the first 13 hours of the 2008 Okmok eruption. One fringe represents along track (approximately north-south) displacement of 10 m. No color variation in the MAI image indicates absent north-south displacement. (b) Histogram of MAI measurements within the rectangular area outlined in Figure 5a. The standard deviation of the MAI measurement is about 15 cm.

that can be achieved with a simple Mogi-type model (see below), we surmise that the 2008 eruption was not fed from a cross-caldera dike or fissure system, but rather from a localized vent or vents along the caldera's ring fracture system.

3. Deformation Modeling and Analysis

3.1. Coeruption Volcano-Wide Subsidence

[12] Earlier geodetic data for Okmok volcano have been modeled using a point source within a homogenous isotropic elastic half-space [e.g., *Mogi*, 1958], which provides a good fit to campaign GPS [*Miyagi et al.*, 2004], CGPS [*Fournier et al.*, 2009] and InSAR data [*Lu et al.*, 1998, 2000, 2005, 2010; *Mann et al.*, 2002]. *Lu et al.* [2010] explored a finite prolate spheroid model for high-quality InSAR images that collectively span the time period 1997–2008 and found that it did not improve the goodness of fit relative to a simpler point source model (i.e., the best fit prolate spheroid was very nearly spherical). We also examined a finite prolate spheroid model for the coeruption deformation source. In the coeruption case, loss of coherence in the near field (i.e., inside the caldera) for most of the InSAR images (Figure 4 and Table 1) makes it difficult to distinguish among source models, none of which produce a significantly better fit than a simple Mogi model. For that reason and given the modeling results for preeruption interferograms, we used only a Mogi model for our subsequent analysis of coeruption interferograms (except for localized intracaldera subsidence revealed by a residual interferogram, see below).

[13] A Mogi source beneath the center of the caldera at a depth of 1.9 ± 0.3 km bsl provides the best fit to the deformation pattern during the first 13 hours of the eruption (Figures 6a–6c). The source location is ~1 km west of that derived from the 1997 coeruption interferogram [*Lu et al.*, 2005], which is consistent with the observation that the average source location migrated westward by ~0.5 km from 1997 to July 2008, prior to the start of the 2008 eruption [*Lu et al.*, 2010]. We do not mean to imply that the magma reservoir as a whole moved laterally either before or during the eruption, but rather that the apparent deformation source shifted progressively over time as a network of interconnected melt bodies and fractures first pressurized and then depressurized (see section 4). The Mogi source volume loss during the first 13 hours of the 2008 eruption was 0.03 km^3, which is about 50% of the volume lost during the entire 1997 eruption.

3.2. Localized Subsidence Within the Caldera

[14] The residual interferogram in Figure 6c (i.e., the difference between observed and modeled interferograms) illustrates the goodness of fit of a Mogi source to the InSAR-derived deformation field for the first 13 hours of the 2008 eruption. Maximum LOS surface displacement during that period was about 76 cm. Only about 3 residual fringes inside the caldera, corresponding to ~15 cm LOS increase (subsidence), are not explained by the best fit Mogi source.

[15] We modeled the residual fringes in Figure 6c using three different sources: Mogi, dike (vertical dislocation, horizontal opening/closing), and tabular source (horizontal dislocation, vertical opening/closing). Our goal was twofold: (1) to understand the cause of localized intracaldera subsidence and (2) to explore further the possibility of dike emplacement during the eruption. The best fit Mogi source is centered ~2 km northeast of Cone A at a depth of ~1.0 km bsl, with a contraction volume of ~0.005 km^3. Figures 6d and 6e show model and residual interferograms for this Mogi source. More than one fringe remains in the residual interferogram, corresponding to ~7 cm LOS displacement (Figure 6e). The variance of the best fit Mogi model is about 2.2 cm^2. Next, we modeled the residual fringes in Figure 6c with an opening vertical dike striking southwest-northeast (i.e., the direction from Cone A to the 2008 vent near

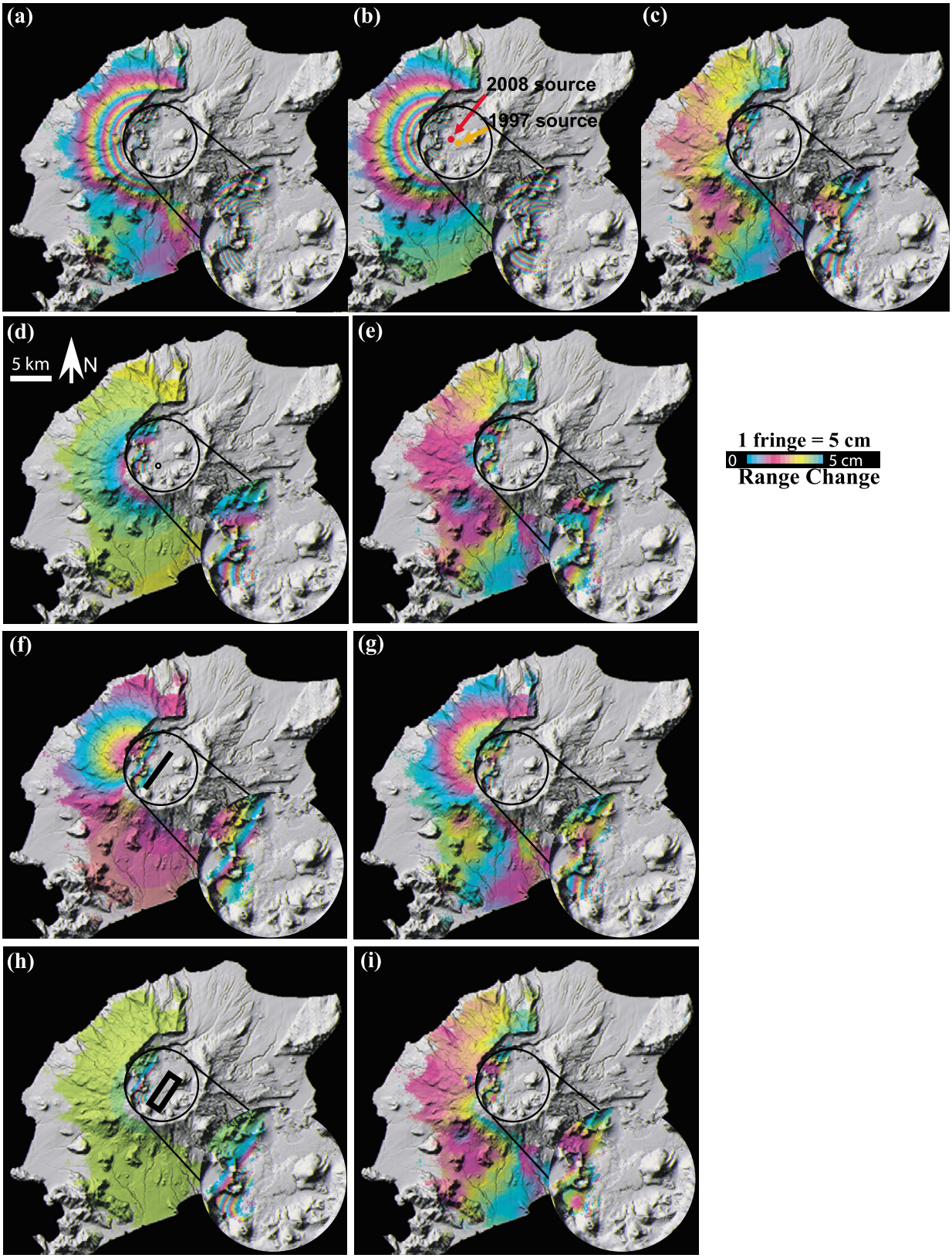
(a)
(b)
2008 source
1997 source
(c)
(d)
5 km
N
(e)
1 fringe = 5 cm
0
5 cm
Range Change
(f)
(g)
(h)
(i)

Figure 6

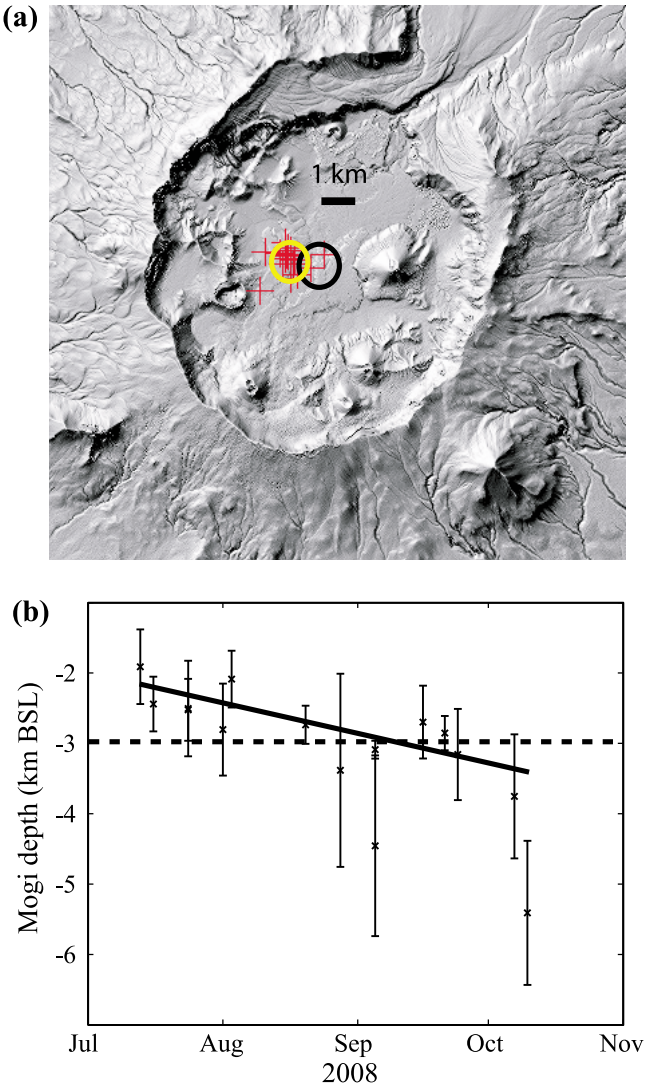

Figure 7. (a) Best fit Mogi source positions (red crosses) from 2008 coeruption interferograms (Table 1), superimposed on a shaded relief image of Okmok caldera. Yellow circle represents the average position of the deformation source for the 2008 eruption. Black circle is the average position of the deformation source both for the 1997 eruption and during the intereruption period 1997–2008. (b) Best fit Mogi source depth as a function of ending date of the interferograms (Table 1). Vertical bar represents one standard deviation of the depth estimate. Thick line is a best weighted linear fit to the depth data as a function of time. Dashed line is the average Mogi source depth from interferograms before the 2008 eruption [*Lu et al.*, 2010].

Cone D). The best model and residual interferograms for a vertical dike source are shown in Figures 6f and 6g, respectively. The variance of the best fit dike model is about 4.7 cm^2, i.e., more than a factor of two worse than the Mogi model. Recall the MAI result and theoretical calculation earlier, which we interpreted to mean that the 2008 eruption was not likely fed by a cross-caldera dike or fissure. Finally, we modeled the residual fringes in Figure 6c using a flat-lying tabular source. The best fit model and residual interferograms are shown in Figures 6h and 6i, respectively. The collapsing tabular source provides the best fit among the three sources investigated, with a variance of ~1 cm^2. The tabular source is located 0.5 km bsl with a contraction volume of 0.005 km^3. The physical interpretation of this result is discussed in the paper's final section.

[16] We modeled the remaining 2008 coeruption interferograms (Table 1) using only a Mogi source, which provided adequate fits to all of the data. Figure 7a shows a compilation of horizontal locations of the best fit Mogi sources derived from all of the individual interferograms. There is no evidence to suggest a change in horizontal position for the 2008 coeruption source during the course of the eruption. The average position of the 2008 coeruption (deflation) source is about 1 km west of: (1) the average position of the 1997 coeruptive (deflation) source, and (2) the average positions of the 1992–1996 and 1997–2008 preeruptive inflation sources [*Lu et al.*, 2010].

[17] Visual inspection of Figure 7b suggests that the model source depth was shallower at the beginning of the 2008 eruption and deepened slightly with time during July–November 2008, an inference that is supported by a weighted least squares linear fit to the data. The best fit line places the mean source depth ~2 km bsl at the beginning of the eruption and ~3 km bsl at the end of the eruption. This result, although not significant at the 95% confidence level, is consistent with a preliminary analysis of CGPS measurements that span the eruption. The CGPS data suggest that the deflation source depth during the 2008 eruption was 0.5–0.7 km shallower than the inflation source depth prior to the start of the eruption [*Freymueller et al.*, 2008].

[18] Magma reservoir volume as a function of time derived from our analysis of 2008 coeruption interferograms (Table 1) is shown in Figure 8. For interferograms with start dates during summer 2008, we added about 0.007 km^3 to account for preeruption inflation during 2007–2008 [*Lu et al.*, 2010]. For interferograms with end dates after the end of the 2008 eruption, there was likely posteruption inflation for which we could not account. The total reservoir volume change associated with the 2008 eruption is 0.14 ± 0.01 km^3, which is ~3 times the result for the 1997 eruption [*Lu et al.*, 2005]. The deflation rate of the reservoir decreased expo-

Figure 6. (a) Observed interferogram of 7 October 2007 to 13 July 2008 (Envisat Track 179), which spans the first 13 hours of the 2008 eruption. (b) Synthetic interferogram corresponding to the best fit Mogi source for the observed interferogram in Figure 6a. (c) Residual interferogram, which is the difference between observed (Figure 6a) and modeled (Figure 6b) interferograms. (d) Synthetic and (e) residual interferograms formed by modeling the residual fringes inside the caldera (Figure 6c) using a contracting Mogi source. (f) Synthetic and (g) residual interferograms formed by modeling the residual fringes in Figure 6c using an opening dike source. (h) Synthetic and (i) residual interferograms formed by modeling the residual fringes in Figure 6c using a contracting horizontal tabular source. One fringe represents a LOS range change of 5 cm to better portray the residual deformation in all. For each InSAR image, deformation inside the caldera is enlarged in the inset to improve visibility.

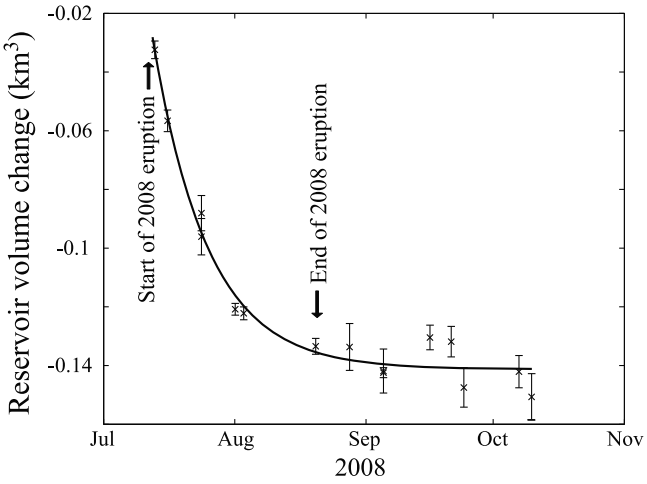

Figure 8. Magma reservoir volume change as a function of time and best fit exponential function (curved line). Error bars represent one standard deviation for volume-change estimates. See text for details.

nentially with time, with a 1/*e* time constant of ~13 days (Figure 8).

4. Discussion

4.1. Implications for Shallow Magma Storage

[19] Our InSAR analysis of Okmok volcano indicates that the source responsible for surface deformation during pre-eruption periods (mostly inflation) was about the same during 1992–1997 and 1998–2008 [*Lu et al.*, 1998, 2000, 2005, 2010; *Mann et al.*, 2002]. We interpret this source as a complex magma storage zone centered ~3.0 km bsl (or ~3.5 km beneath the caldera floor) and extending upward to ~2.0 km bsl. That inference is based on (1) our modeling of high-quality average 1997–2008 interferograms from 9 different satellite tracks, which shows that a nearly spherical source with a radius of ~1 km centered ~3.0 km bsl provides the best fit to preeruption deformation images [*Lu et al.*, 2010]; (2) our modeling results reported in this paper, which suggest that the deflation source depth increased during the course of the 2008 eruption from ~2 km bsl to ~3 km bsl; (3) CGPS results indicating that the average deflation source depth during the 2008 eruption was 0.5–0.7 km shallower than the inflation source depth prior to the eruption [*Freymueller et al.*, 2008]; (4) CGPS data from two stations that operated during the eruption, which suggest deepening of the deflation source with time (J. Freymueller, personal communication, 2009); and (5) recognition that idealized source models with uniformly pressured cavities embedded in homogeneous host rock are abstractions that do not encompass the considerable complexity of the real Earth, particularly beneath volcanoes.

[20] Rather than wholesale vertical migration of a magma-filled cavity over time, we envision progressive pressurization and depressurization of a sponge-like network of interconnected fractures and melt bodies that, in aggregate, constitute the complex magma storage zone beneath Okmok caldera. Apparent deepening of the deflation source during the course of the 2008 eruption plausibly indicates that the reservoir was tapped from the top down, causing a depressurization front to migrate downward as the eruption progressed. InSAR and CGPS data clearly show that the long-term magma supply rate to the reservoir is far less than the eruption rate, so the reservoir is likely to be tapped from the top down during eruptions. This process would manifest itself as progressive deepening of the best fit model source over time, as is the case for the 2008 eruption.

[21] The volume of a spherical cavity with a radius of 1 km is about 4 km^3, which is 3–4 times less than the estimated volumes of the two most recent caldera-forming eruptions at Okmok (~15 km^3 each [*Miller et al.*, 1998; *Finney et al.*, 2008]). Given that the magma reservoir we envision is unlikely to contain 100% melt, it might seem incapable of storing enough magma to explain Okmok's largest eruptions. However, our modeling results are insensitive to the reservoir's bottom depth and not strongly sensitive to reservoir shape, especially at depths greater than a few kilometers. So the apparent discrepancy in volumes can be resolved if parts of the reservoir are deeper than our models can resolve. This would be the case if, as seems likely, the reservoir transitions downward into a vertical feeder system that includes dispersed, partly molten intrusive bodies that might be tapped only during the largest eruptions. Alternatively, the modern reservoir might be smaller than those that fed the two large caldera-forming eruptions.

4.2. Implications for Okmok's Shallow Magma Plumbing System

[22] An obvious question regarding the 2008 eruption is why the eruption site switched from Cone A, which hosted several successive eruptions during the past century and as recently as 1997, to near Cone D which had been inactive for a millennium. Some insight into the reason for the switch might be gleaned from the location of the inflation/deflation source revealed by the interferograms. The magma storage zone is not centered beneath Cone A or Cone D, but beneath the center of the caldera. Considering the depth of the top of the storage zone (~2.5 km below caldera floor) and the diameter of the caldera (10 km), intracaldera vents such as Cone A and Cone D must be fed by dipping magma conduits. The same conduit might be utilized during successive eruptions if it does not become blocked, but eventually a new path of least resistance to the surface would be expected to form. Otherwise, all eruptions would occur from the same summit vent area, as is the case at some volcanoes. Clearly, this is not the case at Okmok, as evidenced by the existence of several dispersed postcaldera vents. So a change in the eruption site between 1997 and 2008, though not anticipated, is not a major surprise. Furthermore there is reason to suspect structural control on magma migration paths from the reservoir to the surface, which would be conducive to shifts in vent location (see below).

[23] The quasi-circular distribution of postcaldera vents within Okmok caldera [*Miller et al.*, 1998; *Grey*, 2003] suggests to us the existence of a ring fracture system that formed during caldera collapse and also played a role in many of Okmok's historical eruptions. We surmise that portions of the ring fracture system episodically serve as a conduit to the surface for magma rising from the subcaldera storage zone. By providing a path of least resistance to

magma flow, the ring fracture system channels most eruptions to sites on the caldera floor, resulting in a series of vents such as Cone A and Cone D. The historical record shows that the same vent area can be active episodically for a long period of time (e.g., eruptions at Cone A in 1943, 1945, 1958, 1960, 1981, 1983, 1986, and 1997), and conversely that the vent location can shift several kilometers along the ring fracture system from one eruption to the next (Cone A in 1997 to near Cone D in 2008). Apparently Okmok's shallow magma plumbing system is distinctly different from those at Hawaiian volcanoes such as Kīlauea and Mauna Loa, where rift zones play a major role in lateral subsurface magma transport beyond the caldera, and intracaldera vent locations seemingly do not align along ring fracture systems.

4.3. Implications for Magma Transport Dynamics

[24] Exponential decay in the 2008 coeruption deflation rate as a function of time is consistent with a hydraulic model in which magma flow rate toward the surface is proportional to the pressure difference between the shallow magma reservoir and vent [*Dvorak and Okamura*, 1987; *Lu et al.*, 2005]. Intuitively, the rate at which the reservoir drains during an eruption is also influenced by magma viscosity and the degree of connectivity within the reservoir. Likewise, the rate of reservoir inflation might be controlled by the pressure difference between a deep magma production zone and the shallow reservoir it supplies. As the reservoir becomes fully engorged prior to an eruption and the pressure difference diminishes, the model predicts that the inflation rate should decline. This is consistent with InSAR observations, which show that the inflation rate at Okmok declined for a few years prior to both the 1997 and 2008 eruptions. Conversely, the pressure difference between a deep source and shallow reservoir is greatest immediately following an eruption, when the model predicts the greatest reservoir inflation rate (e.g., following Okmok's 1997 eruption, as shown by InSAR observations).

4.4. Geodetic Evidence for Groundwater Involvement in the 2008 Eruption

[25] Localized subsidence of the floor of Okmok caldera during the 2008 eruption is evident when the deformation pattern associated with the best fit Mogi source is removed from the observed deformation pattern (Figure 6c). The residual subsidence is best modeled with a flat-lying, collapsing tabular source centered ~0.5 km bsl. We attribute the shallow tabular source to withdrawal of groundwater, which interacted with rising magma to produce the distinctly hydrovolcanic character of the 2008 eruption. Extensive withdrawal of subsurface water would be expected to produce surface collapse, possibly in the form of localized sink holes on the caldera floor. These can be seen in abundance in radar images acquired during the eruption (Figure 1d), and thereafter they were reported by observers in the field [*Larsen et al.*, 2009].

[26] Geodetic data cannot address directly the question of why the 2008 eruption was more explosive than previous historical eruptions at Cone A, but two observations derived from our study are pertinent. The first is InSAR evidence for a shallow collapsing tabular source during the 2008 eruption, which we attribute to groundwater withdrawal. We see no InSAR evidence for a similar source associated with the 1997 eruption at Cone A. In addition, we note from the DEM that the caldera floor drains to the northeast. This drainage pattern makes more surface water, and possibly more groundwater, available for interaction with magma intruding the northeast part of the caldera, where Cone D is located, than the southwest part where Cone A is located. Assuming the drainage pattern has not changed appreciably in the past 1000 years (the age of Cone D), this hypothesis is consistent with the observation by *Larsen et al.* [2009] that prehistoric Cone D deposits suggest highly explosive magma-water interactions.

4.5. Comparison of 1997 and 2008 Eruption Volumes

[27] Our analysis of InSAR imagery indicates that magma storage beneath Okmok decreased by 0.14 ± 0.01 km^3 during the 2008 eruption. This is about 3 times the corresponding decrease during the 1997 eruption (0.05 km^3 [*Lu et al.*, 2005]). The bulk volume of 2008 eruption products is about 0.3 km^3 [*Larsen et al.*, 2009], compared to about 0.15 km^3 for the bulk volume of lava extruded during the 1997 eruption [*Lu et al.*, 2003]. Therefore, bulk volumes for the eruption products are 2–3 times larger than the source volume changes inferred from InSAR modeling. Magma fragmentation during an explosive eruption might account for roughly a factor of two reduction in bulk density (i.e., increase in volume) of ash deposits relative to DRE density, but the same is not true for vesiculation of lava flows during a dominantly effusive eruption. More likely the difference is explained by magma compressibility, which we neglected in our deformation modeling and volume estimates. Magma can be highly compressible under pressure-temperature conditions that prevail in a crustal magma reservoir. A volume increase by a factor of 2–3 is plausible as a result of decompression during magma ascent and eruption [e.g., *Rivalta and Segall*, 2008; *Mastin et al.*, 2008].

4.6. Implications for Magma Supply Rate

[28] The inflation/deflation rate at Okmok was not steady during 1997–2008 [*Lu et al.*, 2010; *Fournier et al.*, 2009], which might indicate that the magma supply from a deep production zone varied with time. Ambiguities imposed by model assumptions, data limitations, and complexities in the real Earth make it difficult to interpret small apparent variations, but the following trends are clear: (1) the Okmok magma reservoir inflated most rapidly immediately after the 1997 eruption; (2) although the preeruption inflation rate might have departed from its long-term trend for periods of a few years (even to the degree that minor deflation seems to have occurred at times), there was an overall tendency for the inflation rate to decline for several years as eruptions approached; and (3) the reservoir deflation rate during eruptions was initially very high, at least an order of magnitude greater than the preeruption inflation rate, and declined exponentially thereafter.

[29] These trends in magma reservoir inflation/deflation cannot be translated directly into magma supply variations, owing to such unknowns as the compressibility of the magma involved and the strength of the reservoir host rock [*Mastin et al.*, 2008]. In the limiting case of very weak host rock and nearly incompressible magma, variations in inflation/deflation rate directly reflect variations in magma sup-

ply rate. This situation is analogous to filling or emptying a water balloon (i.e., a very weak container and a largely incompressible fluid). On the other hand, in the case of very strong host rock and very compressible magma, the relationship between supply rate and inflation/deflation rate is weak, imagine filling or emptying a scuba tank (strong container) with air (highly compressible fluid).

[30] The hydraulic model proposed by *Dvorak and Okamura* [1987] for Kīlauea and invoked by *Lu et al.* [2005] for Okmok approximates the first scenario (weak host rock, relatively incompressible magma). If the model is correct for Okmok, then the InSAR observations reported here and by *Lu et al.* [2010] mean that the magma supply rate to the shallow reservoir beneath the caldera is highest immediately after an eruption and slows thereafter in response to the diminishing pressure gradient between the reservoir and surface. Likewise, the deflation rate during eruptions is greatest initially and declines exponentially. Eventually, supply dominates and a new eruption cycle begins.

[31] It is important to note that we cannot exclude on the basis of the deformation data alone the second scenario, i.e., that the deformation trends described above are more indicative of magma compressibility than variations in magma supply rate. In that case, the magma supply rate could be constant throughout an entire eruption cycle. The reservoir inflation rate would slow prior to an eruption if the host rock were strong enough to resist additional strain, even while highly compressible magma continued to accumulate in the reservoir. This effect would be even greater if the reservoir magma itself were highly compressible. Alternatively the magma supply rate might be variable but not directly coupled to the reservoir inflation rate, which might be more indicative of thermal input to the reservoir or bubble formation, for example.

[32] We can think of two approaches to resolving this ambiguity at Okmok or elsewhere. The first is continuous monitoring of magmatic gas emissions as a proxy for magma supply rate [*Gerlach et al.*, 2002]. The second is coordinated microgravity and deformation measurements to separate the effects of surface height and subsurface mass changes. The two approaches used together throughout an entire eruption cycle should be capable of constraining the true magma supply rate as a function of time.

5. Conclusion

[33] A magma reservoir located beneath Okmok caldera and centered 2–3 km bsl was responsible for volcano-wide deformation from 1992 to 2008, including the 1997 and 2008 eruptions. The reservoir inflated at a rate that was initially high following the 1997 eruption and generally slowed as the 2008 eruption approached. Withdrawal of magma during both eruptions depressurized the reservoir, causing rapid volcano-wide subsidence. Additional localized subsidence occurred within the caldera during the 2008 eruption, which we attribute to collapse of a shallow groundwater lens. Magma began to reaccumulate rapidly in the reservoir soon after the 1997 eruption ended, initiating a new intereruption strain cycle. A hydraulic model in which magma flow rate is proportional to the pressure difference between the reservoir and surface during eruptions, or between a deep production zone and the reservoir between eruptions, can account for the observed patterns of deflation and inflation, respectively. This model could be tested at Okmok or elsewhere with coordinated measurements of gravity, surface height, and gas emission.

[34] We speculate that the caldera ring-fracture system serves as a magma migration pathway from the subcaldera reservoir at Okmok to the surface. Although simple elastic source models do not account for known complexities of the real Earth, they can provide insights into the behavior of real volcanoes. For example, we interpret lateral and vertical migration of the best fit deformation source before and during the 2008 eruption to mean that the reservoir comprises a complex network of interconnected melt bodies and fractures, portions of which pressurize or depressurize differentially over time. Thus, we speculate, the reservoir drains and depressurizes from the top down during eruptions, then fills and repressurizes from the bottom up between eruptions.

[35] For the first time in the Aleutians, InSAR images from 5 different satellite sensors were available for our analysis of the 2008 Okmok eruption, thanks to active tasking of satellites during the eruption. InSAR deformation images were quickly generated, typically within a few days of SAR image acquisition. Until the planned next generation of SAR satellites becomes operational (e.g., NASA's DESDynI, ESA's Sentinel, and Canadian Radarsat-C), we are confident that timely InSAR deformation images and derived models will be available to help diagnose volcano unrest, monitor the progress of eruptions, and support risk mitigation.

[36] **Acknowledgments.** ERS-2 SAR data are copyrighted by the European space Agency (ESA) and were provided by the Alaska Satellite Facility (ASF). Envisat SAR data are copyrighted ESA and were provided by ESA under AOE-567 and CAT1-2765. Some of the 2008 Envisat images were tasked by the UNAVCO Plate Boundary Observatory for the EarthScope Project supported by the U.S. National Science Foundation (EAR-0350028). Radarsat-1 SAR data are copyrighted by the Canadian Space Agency (CSA) and were provided by the Canadian Center for Remote Sensing (CCRS). ALOS SAR data are copyrighted by JAXA/METI and were provided by ASF and JAXA. This work was supported by NASA's Earth Surface and Interiors (ESI) program through grant 2005–0021, and by the USGS Volcano Hazards Program and Land Remote Sensing Program. We thank ESA, ASF, JAXA, and CCRS (B. Brisco) for providing SAR data; C. Wicks for consultation on deformation modeling; H.S. Jung for help with MAI processing; T. Fournier and J. Freymueller for discussion of CGPS data and analysis; and M. Poland, M. Lisowski, and W. Scott for helpful technical reviews. Constructive comments from Associate Editor R. Lohman and two anonymous reviewers have improved the manuscript.

References

Bechor, N. B. D., and H. A. Zebker (2006), Measuring two-dimensional movements using a single InSAR pair, *Geophys. Res. Lett.*, *33*, L16311, doi:10.1029/2006GL026883.

Dvorak, J., and A. T. Okamura (1987), A hydraulic model to explain variations in summit tilt rate at Kilauea and Mauna Loa volcanoes, *U.S. Geol. Surv. Prof. Pap.*, *1350*, 1281–1296.

Finney, B., S. Turner, C. Hawkesworth, J. Larsen, C. Nye, R. George, I. Bindeman, and J. Eichelberger (2008), Magmatic differentiation at an island-arc volcano: Okmok volcano, Aleutian Islands, Alaska, *J. Petrol.*, *49*, 857–884, doi:10.1093/petrology/egn008.

Fournier, T., J. Freymueller, and P. Cervelli (2009), Tracking magma volume recovery at Okmok volcano using GPS and an unscented Kalman filter, *J. Geophys. Res.*, *114*, B02405, doi:10.1029/2008JB005837.

Freymueller, J., T. Fournier, A. Kaufman (2008), Deformation of Okmok volcano associated with its 2008 eruption, *Eos Trans. AGU*, *89*(53), Fall Meet. Suppl., Abstract A53B-0260.

Gerlach, T. M., K. A. McGee, T. Elias, A. J. Sutton, and M. P. Doukas (2002), Carbon dioxide emission rate of Kīlauea volcano: Implications for primary magma and the summit reservoir, *J. Geophys. Res.*, *107*(B9), 2189, doi:10.1029/2001JB000407.

Grey, D. (2003), Post-caldera eruptions at Okmok volcano, Umnak Island, Alaska, with emphasis on recent eruptions from Cone A., M.S. thesis, Univ. of Alaska Fairbanks, Fairbanks, Alaska.

Jung, H. S., J. S. Won, and S. W. Kim (2009), An improvement of the performance of multiple aperture SAR interferometry (MAI), *IEEE Trans. Geosci. Remote Sens.*, *47*, 2859–2869, doi:10.1109/TGRS.2009.2016554.

Jung, H. S., Z. Lu, J. S. Won, M. P. Poland, and A. Miklius (2010), Mapping three-dimensional surface deformation by combining multiple aperture interferometry and conventional interferometry: Application to the June 2007 eruption at the Kilauea volcano, Hawaii, *IEEE Geosci. Remote Sens. Lett.*, in press.

Larsen, J., C. Neal, P. Webley, J. Freymueller, M. Haney, S. McNutt, D. Schneider, S. Prejean, J. Schaefer, and R. Wessels (2009), Eruption of Alaska volcano breaks historic pattern, *Eos Trans. AGU*, *90*(20), 173–175, doi:10.1029/2009EO200001.

Lu, Z., D. Mann, and J. Freymueller (1998), Satellite radar interferometry measures deformation at Okmok Volcano, *Eos Trans. AGU*, *79*(39), 461–468, doi:10.1029/98EO00348.

Lu, Z., D. Mann, J. Freymueller, and D. Meyer (2000), Synthetic aperture radar interferometry of Okmok volcano, Alaska: Radar observations, *J. Geophys. Res.*, *105*, 10,791–10,806, doi:10.1029/2000JB900034.

Lu, Z., E. Fielding, M. Patrick, and C. Trautwein (2003), Estimating lava volume by precision combination of multiple baseline spaceborne and airborne interferometric synthetic aperture radar: The 1997 eruption of Okmok volcano, Alaska, *IEEE Trans. Geosci. Remote Sens.*, *41*(6), 1428–1436, doi:10.1109/TGRS.2003.811553.

Lu, Z., T. Masterlark, and D. Dzurisin (2005), Interferometric synthetic aperture radar study of Okmok volcano, Alaska, 1992–2003: Magma supply dynamics and post-emplacement lava flow deformation, *J. Geophys. Res.*, *110*, B02403, doi:10.1029/2004JB003148.

Lu, Z., D. Dzurisin, J. Biggs, C. Wicks, and S. McNutt (2010), Ground surface deformation patterns, magma supply, and magma storage at Okmok volcano, Alaska, inferred from InSAR analysis: 1. Intereruption deformation between 1997 and 2008, *J. Geophys. Res.*, *115*, B00B02, doi:10.1029/2009JB006969.

Mann, D., J. Freymueller, and Z. Lu (2002), Deformation associated with the 1997 eruption of Okmok volcano, Alaska, *J. Geophys. Res.*, *107*(B4), 2072, doi:10.1029/2001JB000163.

Massonnet, D., and K. Feigl (1998), Radar interferometry and its application to changes in the Earth's surface, *Rev. Geophys.*, *36*, 441–500, doi:10.1029/97RG03139.

Mastin, L., E. Roeloffs, N. Beeler, and J. Quick (2008), Constraints on the size, overpressure, and volatile content of the Mount St. Helens magma system from geodetic and dome-growth measurements during the 2004–2006 eruption, *U.S. Geol. Surv. Prof. Pap.*, *1750*, 461–488.

Miller, T. P., R. G. McGimsey, D. H. Richter, J. R. Riehle, C. J. Nye, M. E. Yount, and J. A. Dumoulin (1998), Catalog of the historically active volcanoes of Alaska, *U.S. Geol. Surv. Open-File Rep. 98-582*, 104 p.

Miyagi, Y., J. Freymueller, F. Kimata, T. Sato, and D. Mann (2004), Surface deformation caused by shallow magmatic activity at Okmok volcano, Alaska, detected by GPS campaigns 2000–2002, *Earth Planets Space*, *56*, e29–e32.

Mogi, K. (1958), Relations between the eruptions of various volcanoes and the deformations of the ground surface around them, *Bull. Earthquake Res. Inst. Univ. Tokyo*, *36*, 99–134.

Rivalta, E., and P. Segall (2008), Magma compressibility and the missing source for some dike intrusions, *Geophys. Res. Lett.*, *35*, L04306, doi:10.1029/2007GL032521.

Rosen, P. A., S. Hensley, I. Joughin, F. Li, S. Madsen, E. Rodriguez, and R. Goldstein (2000), Synthetic aperture radar interferometry, *Proc. IEEE*, *88*, 333–380, doi:10.1109/5.838084.

Sandwell, D., D. Myer, R. Mellors, M. Shimada, B. Brooks, and J. Foster (2008), Accuracy and resolution of ALOS interferometry: Vector deformation maps of the Father's day intrusion at Kilauea, *IEEE Trans. Geosci. Remote Sens.*, *46*(11), 3524–3534, doi:10.1109/TGRS.2008.2000634.

Zebker, H. A., P. A. Rosen, R. M. Goldstein, A. Gabriel, and C. L. Werner (1994), On the derivation of coseismic displacement fields using differential radar interferometry: The Landers earthquake, *J. Geophys. Res.*, *99*(B10), 19,617–19,634, doi:10.1029/94JB01179.

D. Dzurisin and Z. Lu, Cascades Volcano Observatory, U.S. Geological Survey, 1300 SE Cardinal Ct., Building 10, Suite 100, Vancouver, WA 98683-9589, USA. (lu@usgs.gov)